ACS OMEGA

http://pubs.acs.org/journal/acsodf

Article

Facile Gram-Scale Synthesis of NiO Nanoflowers for Highly Selective and Sensitive Electrocatalytic Detection of Hydrazine

Rayse M. Ferreira, Franciele M. Morawski, Emanuel C. Pessanha, Scarllett L. S. de Lima, Diana S. da Costa, Geyse A. C. Ribeiro, João Vaz, Rodolpho Mouta, Auro A. Tanaka, Liying Liu, Maria I. P. da Silva, Aryane Tofanello, Hector A. Vitorino, Anderson G. M. da Silva,* and Marco A. S. Garcia*

Cite This: *ACS Omega* 2023, 8, 11978−11986

Read Online

ACCESS | Metrics & More | Article Recommendations | Supporting Information

ABSTRACT: The design and development of efficient and electrocatalytic sensitive nickel oxide nanomaterials have attracted attention as they are considered cost-effective, stable, and abundant electrocatalytic sensors. However, although innumerable electrocatalysts have been reported, their large-scale production with the same activity and sensitivity remains challenging. In this study, we report a simple protocol for the gram-scale synthesis of uniform NiO nanoflowers (approximately 1.75 g) via a hydrothermal method for highly selective and sensitive electrocatalytic detection of hydrazine. The resultant material was characterized by scanning electron microscopy, X-ray photoelectron spectroscopy, and X-ray diffraction. For the production of the modified electrode, NiO nanoflowers were dispersed in Nafion and drop-cast onto the surface of a glassy carbon electrode (NiO NF/GCE). By cyclic voltammetry, it was possible to observe the excellent performance of the modified electrode toward hydrazine oxidation in alkaline media, providing an oxidation overpotential of only +0.08 V vs Ag/AgCl. In these conditions, the peak current response increased linearly with hydrazine concentration ranging from 0.99 to 98.13 μmol L^{-1}. The electrocatalytic sensor showed a high sensitivity value of 0.10866 μA L μmol^{-1}. The limits of detection and quantification were 0.026 and 0.0898 μmol L^{-1}, respectively. Considering these results, NiO nanoflowers can be regarded as promising surfaces for the electrochemical determination of hydrazine, providing interesting features to explore in the electrocatalytic sensor field.

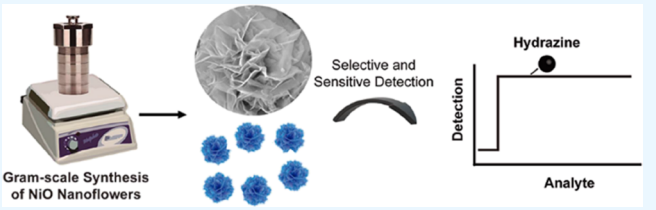

INTRODUCTION

Electrocatalytic nanomaterials have been a topic of research in the frontiers of electrochemistry, which includes their utilization in advanced applications, such as oxidation of environmental pollutants, non-enzymatic determination of organic compounds, and efficient design of fuel cells, supercapacitors, and batteries, among others.[1−9] Mainly, nanostructured metal oxides based on copper, nickel, and zinc are efficient electrocatalysts when considering non-noble precursors;[10−12] thus, materials based on these oxides are highly studied. Also, although some oxides find specific utilization, many applications are mutual.[13] Therefore, with the emergence of nanotechnology, the performance of metal oxides is not exclusively based on their chemical nature; instead, their properties can be tuned by controlling several parameters, including size, shape (surface facets), composition, and structure.[14−18] From this perspective, producing nanocavities over materials or obtaining nanocubes, nanowires, nanorods, nanosheets, and nanoflower-based metal oxides can provide advanced surface features for creating electrocatalytic sensors.[12,19−22] Among the different morphologies cited before, nanoflowers showing structural similarity to real flowers have attracted increased interest nowadays since they are composed of several thin layers of petals forming a highly porous structure encompassing a larger surface area and highly active surface sites for multiple applications in catalysis, sensors, and delivery of drugs.[23−26]

In light of the foregoing, metal oxide utilization reaches a new level once fine manipulations highly affect their performance, which sometimes makes it difficult to choose a potential candidate for a specific application. However, some considerations regarding the previous literature may help in its task. Thus, nickel oxide (NiO) nanostructured electrocatalysts are especially attractive due to their high activity, sensitivity, precursors' abundance, and lower cost when compared to noble-metal electrocatalytic sensors.[13] Also, from a physicochemical perspective, NiO presents other features that make it suitable for consideration regarding sensing applications: (1)

Received: November 29, 2022
Accepted: February 7, 2023
Published: March 21, 2023

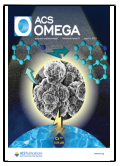

ease of obtaining several morphologies, which, generally, affords high surface area and porosity, improving their results;[27−34] (2) tunable electrical conductivity by controlling microstructural defects such as vacancies and interstitials;[35] (3) high electrochemical and structural stability of nickel and nickel-based mixed oxides[36,37] and; (4) preparation of stable NiO with just one phase, improving the fast transfer of electrons between Ni^{2+} and Ni^{+} species when required.[38] Such features make NiO nanomaterials highly promising for applications in supercapacitors,[39] renewable energy,[40] and non-enzymatic glucose sensing.[41] For electrochemical sensors, modified Ni, NiO, and $Ni(OH)_2$ electrodes commonly provide a well-known redox peak in basic media, which can be related to the oxyhydroxide NiOOH species.[42] In these conditions, nickel oxide can be explored for the catalytic oxidation of many molecules, including glucose and hydrazine.[43] The main focus is to reduce the redox overpotential, enabling the production of selective and sensitive electrocatalytic sensors. However, despite several successful attempts to synthesize NiO nanoflowers, most reported protocols are usually restricted by the low amounts of produced materials (limited to milligrams) or do not display uniform sizes and shapes.[44−47] In particular, anisotropic NiO nanomaterials have attracted significant attention in catalysis, sensor, and plasmonics[48] for the following reasons: (i) higher specific surface areas relative to those of commercial samples, (ii) crystal growth along high index facet and high surface energy, leading to highly catalytically active crystallographic directions, (iii) easily accessible surface by gas and liquid substrates due to their porous structures, and (iv) diminished sintering processes, which generally are responsible for significant decreases in the surface area of several catalysts and can be significantly retarded in anisotropic nanomaterials as compared to other shapes. Thus, obtaining high quantities of such materials in a controlled shape is highly interesting.

Undeniably, electrocatalytic oxidation of hydrazine (N_2H_4) is an interesting research topic with technological use in alternative energy production and high-performance sensor devices.[41,49] Hydrazine is a key inorganic compound mainly used in the chemical industry with undisputable properties as a catalyst, reducing, and foaming agent. It is also used as an intermediate of synthetic routes to produce pesticides, polymers, and pharmaceuticals.[50−52] This compound has triggered technological inventions such as rocket fuels and car airbags because of its propellant properties.[33] Despite its excellent features, hydrazine is carcinogenic, and high exposition levels can lead to several adverse effects on human health.[53,54] Aware of this harmful characteristic of hydrazine, some oxides have been proposed to promote the catalytic oxidation of this compound, with an emphasis on NiO. While many works have focused on investigating mixed nickel oxide materials to improve sensor performance (AuNPs-NiO, MWCNT-NiO, and NiO/CuO),[55−57] only a few have explored their shape-dependent intrinsic properties.

Here, we provide the simple and fast one-step gram-scale synthesis of hierarchically structured nickel oxide nanoflowers (NiO NF) for electrochemical sensing of hydrazine. The produced NiO NF was characterized by different techniques, including scanning electron microscopy (SEM), high-resolution transmission electron microscopy (HRTEM), X-ray diffraction (XRD), and X-ray photoelectron microscopy (XPS). The resultant material was dispersed in Nafion and employed to produce a modified glassy carbon electrode (NiO NF/GCE). Cyclic voltammetry in alkaline media was used to investigate the electrochemical performance of NiO NF toward hydrazine oxidation to develop a highly sensitive and selective electrocatalytic sensor.

EXPERIMENTAL SECTION

Materials and Instrumentation. Analytical-grade nickel(II) chloride hexahydrate ($NiCl_2{\cdot}6H_2O$, ≥ 98%), sodium dodecyl sulfonate (SDS, ≥ 99%), urea (≥ 99.5%), potassium hydroxide (90%), and hydrazine sulfate (≥ 99%) were purchased from Sigma-Aldrich and used without further purification. The solutions were prepared with deionized water (resistivity of 18.2 MΩ cm, Millipore , Billerica, USA).

SEM images were acquired in a JEOL field emission gun microscope JSM 6330F (JEOL, Tokyo, Japan), operated at 5 kV. The HRTEM images were obtained with a JEOL JEM 2100 microscope (JEOL, Tokyo, Japan) operated at 200 kV. For sample preparation, 0.01 g of the material was dispersed in 10 mL of deionized water and sonicated with an ultrasonic bath to suspend the material in the solvent. Then, the aqueous suspension containing the nanostructures was drop-cast over a silicon wafer (for SEM analysis) or a carbon-coated copper grid (for HRTEM analysis), followed by drying under ambient conditions.

XPS analyses were performed with a K-Alpha X-ray photoelectron spectrometer system. The calibration used the C 1s peak (BE = 284.8 eV). CasaXPS processing software version 2.3.15 (Casa Software Ltd., Teignmouth, UK) was used for data analysis. XRD analyses were performed using a Bruker D8 Advance diffractometer. The scans were recorded in the 2θ range between 10 and 85°. The phase composition was determined by Rietveld refinement using GSAS-II software. Textural characteristics for the catalysts were determined from nitrogen adsorption isotherms, recorded at −196 °C in a Micromeritics (Norcross, GA) Gemini III 2375 surface area analyzer. The samples (ca. 100 mg) were degassed for 3 h at 150 °C before analysis. The BET method determined specific surface areas from the adsorption isotherm generated in a relative pressure range of $0.07 < P/P_o < 0.3$.

Gram-Scale Synthesis of NiO Nanoflowers. The gram-scale synthesis of NiO nanoflowers was performed by a hydrothermal method in a batch-stirred high-pressure reactor system (Berghof BR-500, Eningen unter Achalm, Germany) with a 500 mL PTFE-lined vessel employed. In a typical experiment, two solutions were first prepared: (1) 150 mL of an aqueous solution of SDS (4.33 g) and (2) 150 mL (75 mL of water and 75 mL of ethanol) of $NiCl_2{\cdot}6H_2O$ (7.13 g) and urea (9.0 g). Then, solution (1) was dropwise added to solution (2) and stirred for 30 min at room temperature before transfer to a 500 mL Berghof BR-500, which was kept at 120 °C for 12 h. The resultant solid was washed with deionized water and ethanol several times and dried at 60 °C under atmosphere conditions for 10 h. Lastly, the product was calcined at 350 °C for 2 h under air atmosphere. The material was designated as NiO nanoflowers. The complete production of NiO nanoflowers is summarized in Scheme 1.

Electrochemical Measurements. The measurements were performed using an Autolab PGSTAT302N potentiostat (Metrohm, Netherlands) connected to a computer with NOVA 2.1.4 software. A three-electrode electrochemical cell was used, in which the reference, auxiliary, and working electrodes were AglAgCllKCl$_{sat}$, Pt, and glassy carbon (GC, A = 0.196 cm^2) modified with the prepared material, respectively.

https://doi.org/10.1021/acsomega.2c07638
ACS Omega 2023, 8, 11978−11986

Scheme 1. Illustrative Synthetic Route for the Production of NiO Nanoflowers

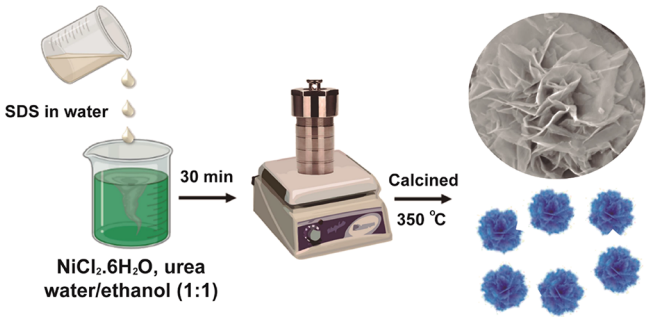

The GC electrode was polished with alumina slurry (0.3 and 0.05 μm, Buehler) and then further cleaned under ultrasound for 5 min using a mixture of water and ethanol (2:1). The NiO nanoflower suspension was prepared by mixing 2.0 mg of the material, 950 μL of deionized water, and 50 μL of Nafion 5.0 wt %[58] and kept under ultrasound for 1 h. Then, 20 μL of the suspension was dropped onto the GC surface and left to dry under ambient conditions. The measurements were performed using freshly prepared 0.1 mol L^{-1} KOH and 1.0 mmol L^{-1} hydrazine. The calibration plots were constructed by the standard addition method.

The real sample analysis used tap water (from the laboratory), which was diluted without further purification with 0.1 mol L^{-1} KOH with a 1:4 dilution. After this, different hydrazine concentrations were added to the sample and analyzed with the standard addition method.[59]

Amperometry measurements were performed by setting the modified working electrode to different concentrations of hydrazine; a hydrodynamic study was carried out in the presence of 50 μmol L^{-1} of hydrazine, varying the potentials (−0.10, −0.05, 0.00, 0.05, 0.10, 0.15, 0.20, 0.25, and 0.35 V). The limit of quantification (LOQ) and the limit of detection (LOD) were estimated using the following equations:[60]

$$\mathrm{LOQ} = \frac{10\sigma}{s}$$

$$\mathrm{LOD} = \frac{3\sigma}{s}$$

where s is the slope of the calibration curve and σ is the standard deviation of the linear coefficient.

RESULTS AND DISCUSSION

In this study, we decided to synthesize a hierarchical nickel-based material with a high surface-to-volume ratio to exploit its properties via a simple, scalable, viable, and cost-effective hydrothermal method. On this basis, the characteristics raised from hierarchical structures are expected to provide faster electron transfer and sensitivity, essential features for electrochemical sensors.[38] Therefore, the investigations started with the gram-scale synthesis of NiO nanoflowers. Our approach enabled their synthesis on a gram scale (approximately 1.75 grams of nanoflowers) and using inexpensive reactants (as described in the Experimental section).

Figure 1A−C shows SEM images in different magnifications, showing that the nanoflowers displayed well-defined shapes and uniform sizes, with petals being 15 ± 8 nm in width and >1 μm in diameter (each nanoflower holds approximately 15

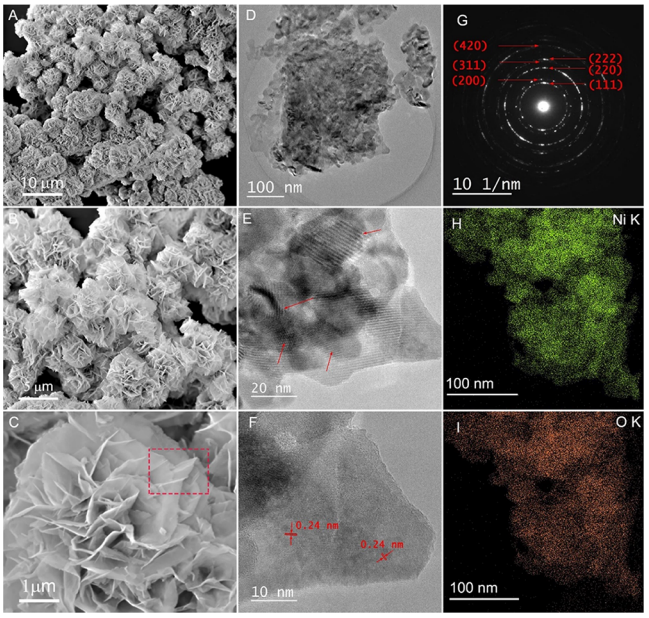

Figure 1. SEM images of the NiO NF at different magnifications (A−C), low-magnification TEM image (D). HRTEM image with Moiré fringes marked by the arrows (E). HRTEM image with the spacing between the atomic planes of 0.24 nm, corresponding to the d value of (111) planes (F). The selected area diffraction pattern of image (D) with the structures indexed (G). The index was done with the PDF card's standard powder X-ray diffraction pattern (code 00-001-1239). STEM-EDS elemental mapping of Ni (H) and O (I).

petals). In addition, visible boundaries in the material suggest a growth mechanism of particle attachment.[61] This could be confirmed through the images of TEM (Figure 1D) and HRTEM (Figure 1E,F). It was possible to observe that a particle attachment forms the NiO nanoflowers following a self-assembly process. The selected area electron diffraction (SAED) pattern of NiO nanoflowers (Figure 1G) showed that the nanomaterial is polycrystalline. In addition, STEM-EDS elemental mapping (Figure 1H,I) confirmed the uniform distribution of Ni and O at the NiO nanoflower surface.

Although the nanoflowers were successfully prepared, a pure crystal phase is required to associate its electrochemical performance with its structure. Therefore, we used the Rietveld refinement method to construct diffraction patterns calculated according to a crystallographic standard model.[62] The experimental XRD pattern was adjusted to a Rietveld routine to provide structural parameters of the as-prepared material (Figure 2). The refinement confirmed the presence of NiO crystals with a pure phase (there were no diffraction peaks of other impurities), as aimed by the synthesis (R_{wp} = 2.19% e

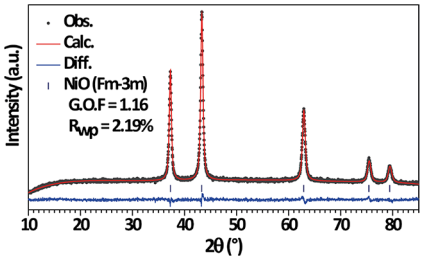

Figure 2. Rietveld refinement plot for the NiO NF showing the observed, calculated, and difference between X-ray patterns.

https://doi.org/10.1021/acsomega.2c07638
ACS Omega 2023, 8, 11978−11986

G.O.F = 1.16). The diffraction peaks could be well indexed to the cubic-type structure, with a space group of Fm-3m and lattice parameter and microstrain of 4.178 Å e 8.2 × 10^{-3}, respectively, exhibiting high crystallinity of the NiO phase.

Once a pure phase was achieved, the surface electronic state and surface analysis of the material was further investigated by XPS to characterize the material further. Thus, the survey spectrum confirms the presence of Ni, O, and C without interferents (not shown). The high-resolution spectra of Ni 2p exhibit two major peaks at 871.7 and 854.2 eV, attributed to the orbital splitting level of Ni $2p_{1/2}$ and Ni $2p_{3/2}$, respectively.[63] As shown in Figure 3A, the Ni 2p profile for

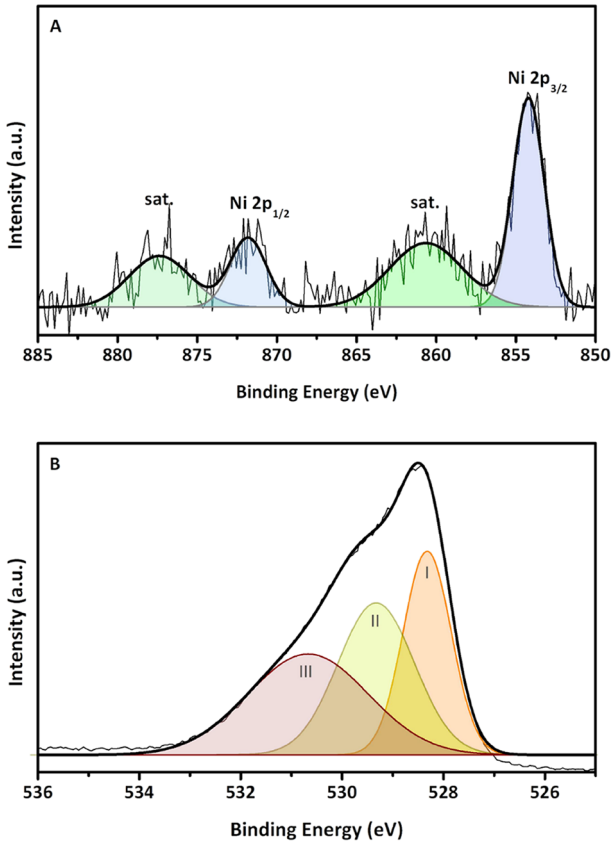

Figure 3. (A) Ni and (B) O XPS high-energy resolution spectra of the NiO NF.

the structure showed an orbital energy separation with a difference of 17.6 eV, which confirms that the oxidation state of the Ni ion exists in a 2+ valence state.[64] In addition, two shake-up satellite peaks were observed at 877.3 and 860.7 eV, assigned to Ni $2p_{1/2}$ and Ni $2p_{3/2}$, respectively.[65]

Furthermore, high-resolution spectra of O 1p revealed three peaks at 528.3, 529.3, and 530.7 eV for the O 1s spectrum (highlighted as I, II, and III in Figure 3B). The first one, at 528.3 eV, can be attributed to the nucleophilic oxygen species and typically indicates the presence of chemisorbed oxygen (hydroxide binding). The binding energy peak at 529.3 eV was ascribed to the typical metal-oxygen bond (lattice oxygen) of Ni−O. The last peak, at 530.7 eV, could be related to the defective nickel oxide (oxygen vacancy).[66]

In the next step, to estimate the electrochemical performance of NiO NF/GCE, cyclic voltammetry studies were performed in the presence of hydrazine 1 mmol L^{-1} at a scan rate of 50 mV s^{-1} using KOH 0.1 mol L^{-1} as the supporting electrolyte, as shown in Figure 4. There were no apparent

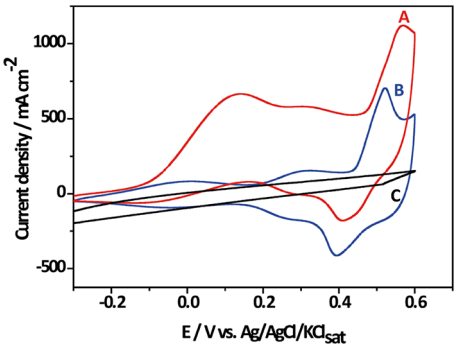

Figure 4. CV curves performed in 0.1 M KOH at the scan rate of 50 mV s^{-1} of the bare (A) GC electrode, (B) NiO NF/GCE electrode, and (C) NiO NF/GCE electrode in the presence of 1 mmol L^{-1} of hydrazine.

redox peaks for the bare GCE, when the electrode was interrogated in the presence of hydrazine 1 mmol L^{-1} in alkaline media (curve A, black line). This result agrees with the previous report, showing that hydrazine oxidation does not occur on non-activated bare GCE surfaces.[67] Thus, the electrochemical oxidation of hydrazine requires the use of electrocatalytic modifiers to reduce its oxidation overpotential.

To evaluate the response of novel NiO NF/GCE, the electrode response was first investigated in the absence of hydrazine (curve B, blue line). According to the literature, NiO on the surface tends to form surface-$Ni(OH)_2$ immediately, when the electrode is placed in alkaline media. CV measurements of NiO NF/GCE were recorded in KOH 0.1 mol L^{-1} using a potential range from −0.3 to +0.6 V vs Ag/AgCl. In these conditions, it was possible to identify an improvement of the faradaic and capacitive currents with a typical oxidation peak near +0.3 and +0.5 V vs Ag/AgCl, which can be associated with the formation of NiO(OH) in basic solution (curve B).[68] Basically, the formation of $Ni(OH)_2$ proceeds through three consecutive steps: the discharge of OH^- anions at the metal surface and the formation of the adsorbed OH species (Ni-OH_{ad}), the incorporation of OH into "intermediary surface" or subsurface between the first and the second layer of Ni atoms, and chemisorption of the second monolayer of OH groups on the (OHNi) subsurface. According to the literature, it can be explained due to the redox process of Ni^{2+}/Ni^{3+}, which is presented in eq 1. Also, the appearance of two oxidation peaks suggests the phase transformation from β-NiO(OH) to γ-NiO(OH).[69]

$$Ni(OH)_2 + OH^- \rightarrow NiO(OH) + e^- \quad (1)$$

$$N_2H_4 + 4\,NiO(OH) \rightarrow N_2 + 4H_2O + 4e^- + NiO \quad (2)$$

After hydrazine addition, it was possible to notice the appearance of an irreversible oxidation peak near +0.08 V vs Ag/AgCl that presented a current density of 671 μA cm^{-2} (curve C, red line). This signal can be associated with hydrazine oxidation in the presence of OH^- species, producing N_2 and H_2O, as illustrated in eq 2.[69] A possible oxidation mechanism can be associated with NiO(OH) production onto the electrode surface. The adsorbed OH^- localized on the 3d orbital of Ni will subsequently participate in hydrazine oxidation to produce N_2 and H_2O.[56] In a possible mechanism,

https://doi.org/10.1021/acsomega.2c07638
ACS Omega 2023, 8, 11978−11986

the electrocatalytic cycle is completed with the oxidation of hydrazine, which delivers free NiO nanoflowers onto the electrode surface, as shown in eq 2.

Due to their several thin layers of petals forming an irregular, rough, and porous structure, NiO nanoflowers are expected to provide an increased number of active sites for the electrocatalytic oxidation of hydrazine, explaining the superior performance of this material. Such a proposition is confirmed by the textural properties of the NiO nanoflowers obtained by N_2 adsorption (BET method). NiO nanowires presented a much higher specific surface area (42 m^2 g^{-1}) than commercial NiO (9 m^2 g^{-1}), as observed in Figure S1. Compared to previous work, the proposed NiO NF/GCE requires only +0.08 V vs Ag/AgCl for hydrazine oxidation, whether similar reactions occur at +0.87 V vs Ag/AgCl, even in the presence of highly ordered metallic oxide materials.[70] The peak current improvement and the low oxidation overpotential of hydrazine suggest the excellent electrocatalytic behavior of the proposed NiO NF/GCE.

CV at different scan rates provides important details of the redox mechanisms at different modified electrode surfaces, allowing to study the adsorption and/or diffusion redox mechanisms. From this perspective, the NiO NF/GCE was tested at different scan rates from 10 to 100 mV s^{-1} in the presence of hydrazine 1 mmol L^{-1} in alkaline media KOH 0.1 mol L^{-1}. CV recorded at different scan rates are presented in Figure 5A. From the voltammograms, it was possible to observe a linear behavior between hydrazine anodic peak current (I_{pa}) and the square root of scan rate ($\upsilon^{1/2}$), as seen in Figure 5B. The linear dependence can be expressed as $I/\mu A\ cm^{-2} = 5.13\ \upsilon^{1/2} + 9.87$ with a correlation coefficient of 0.999. According to the Randles-Sevick equation, this linear dependence indicates a typical diffusion-controlled redox reaction

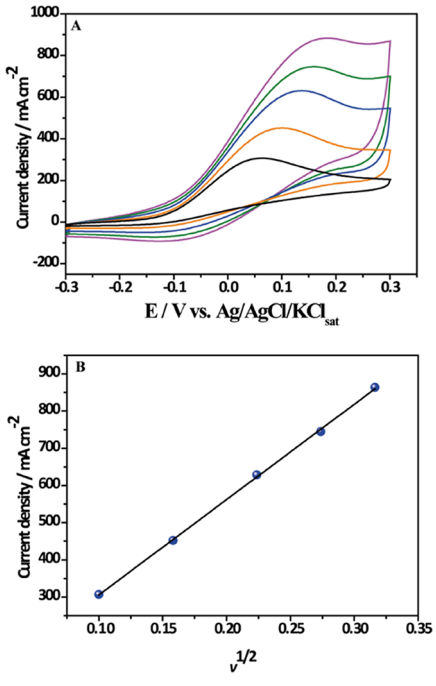

Figure 5. (A) CV of the NiO NF/GCE electrode recorded at different rates in 0.1 mol L^{-1} KOH solution containing 1.0 mol L^{-1} hydrazine at room temperature. (B) Graph of dependence of the peak current (I_p) with the square root of the sweep speed of the potential for hydrazine oxidation on the modified electrode.

onto the electrode/solution interface. This result suggests a faster electron transfer redox reaction led by the diffusion of hydrazine species from the bulk to the electrode surface.[50]

Finally, to investigate the analytical applicability of NiO NF/GCE for the electrochemical determination of hydrazine, CV experiments were performed in the presence of a different concentration of the analyte in KOH 0.1 mol L^{-1} at 50 mV s^{-1}. Figure 6A shows the voltammograms for successive additions

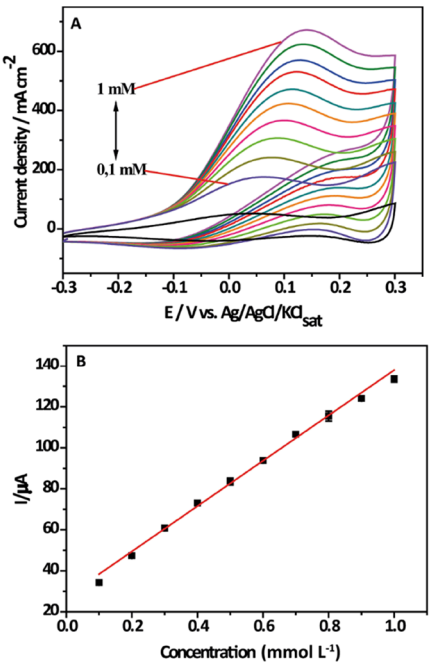

Figure 6. (A) CV of NiO NF/GCE performed in the presence of different concentrations of hydrazine 0.1−1 mmol L^{-1} in KOH 0.1 mol L^{-1} at 50 mVs^{-1}. (B) Linear dependence between $\mu A\ cm^{-2}$ vs Hydrazine concentration.

of hydrazine. The increase of the oxidation peak at +0.08 V vs Ag/AgCl is proportional to the increase of analyte concentration in a range from 0.1 to 1 mmol L^{-1}. Figure 6B presents the linear dependence between the anodic peak current density and hydrazine concentration that can be expressed by $I/\mu A\ cm^2 = 137 + 547$ [hydrazine] mmol L^{-1} with a correlation coefficient of 0.998.

The calibration plots obtained sensitivity and intercept deviation values were 547 $\mu A\ cm^{-2}$ mmol L^{-1} and 137 $\mu A\ cm^{-2}$, respectively. The limit of detection and limit of quantification were statistically calculated based on the IUPAC recommendations as 3 × SD/slope and 10 × SD/slope, respectively. For this purpose, SD was considered as the standard deviation of blank measurements (n = 10). The estimated values were 10.8 e 30.6 μmol L^{-1} for LOD and LOQ, respectively. According to the United States Environmental Protection Agency (EPA), the maximum residue level of hydrazine in effluents is 1 ppm.[50] This value corresponds to 31 μmol L^{-1}. Since the LOD and LOQ are in the range of the required MRL values, the proposed sensor presents promising features for hydrazine monitoring in environmental samples. Also, the low oxidation overpotential ensures a high selectivity for this method once only a few organic molecules can undergo oxidation reactions in the applied potential range. Table 1 summarizes the sensor performance of NiO NF/GCE for hydrazine oxidation.

https://doi.org/10.1021/acsomega.2c07638
ACS Omega 2023, 8, 11978−11986

Table 1. Parameters Evaluated for the NiO NF/GCE in the Presence of Hydrazine

linear range	100−1000 μmol L^{-1}
intercept	157.3 μA cm^{-2}
slope	547 μA cm^{-2} mmol L^{-1}
correlation coefficient	0.998
limit of detection	10.0 μmol L^{-1}
limit of quantification	30.6 μmol L^{-1}

Data obtained from the literature were used to estimate the electrochemical performance of NiO NF/GCE compared to other electrode materials. Table 2 shows comparative results of oxidation overpotential, electrolyte solution, linear range, and sensitivity of NiO nanoflowers and other reported materials for hydrazine oxidation. Interestingly, the NiO NF/GCE provided a low hydrazine oxidation overpotential, highlighting the excellent electrocatalytic behavior of NiO nanoflowers. Indeed, this result improves the selectivity toward hydrazine determination, avoiding the overlap of redox reactions of other molecules that commonly occur in higher overpotentials. Another key point of NiO NF/GCE performance was the sensor sensitivity, which was higher than other electrocatalytic materials based on nickel, gold, cobalt, and gold nanostructures. For example, the sensor showed a 4-fold improvement in sensitivity compared to β-Nickel hydroxide nanoplatelet-modified electrode (Ni-NP).[52] This result indicates the high performance and promising application of the NiO nanoflowers for hydrazine sensing. Additionally, the sensor showed an adequate linear range, suggesting possible analytical application in environmental sensing.

Amperometry measurements were taken at the same concentration of hydrazine, in which a hydrodynamic study was used to optimize the applied potential. According to Figure S2, the results suggested that the optimal potential is 150 mV, which allows for better results from hydrazine's electro-oxidation on the surface of the NiO NF electrode. Figure S3A shows the amperometry curves for the determination of hydrazine in different concentrations (0.99−98.13 μmol L^{-1}), in which it is possible to observe a linear dependence of the hydrazine oxidation peak current, regarding the concentration. The corresponding calibration curve (Figure S3B) shows the linear current increase with a rise in hydrazine concentration. The linear equation obtained was I (μA) = 0.10866[hydrazine (μmol L^{-1})] + 0.01155, and the correlation coefficient was estimated at 0.999. The LOQ and the LOD were 0.0898 and 0.026 μmol L^{-1}, respectively.

Then, a selectivity study was performed in the presence of possible interfering agents (K^+, Cl^-, Na^{2+}, PO_4^{2-}, and urea) at a concentration ratio of 1:1 in 0.1 mol L^{-1} KOH solution in the presence of 30 μmol L^{-1} of hydrazine. Figure S4A shows amperometry curves, in which it was observed that the addition of these interfering species did not show a considerable change in the current signals for hydrazine oxidation. As seen in Figure S4B, the results show high selectivity, with a response variation for hydrazine of less than 9%.

In this scenario, the applicability of the proposed system was investigated in a real sample with tap water (Figure S5). Due to the high selectivity demonstrated by the modified electrode, no previous treatment was necessary; only a dilution of the sample in KOH 0.1 mol L^{-1} support the electrolyte before the analysis. Addition and recovery measurements were conducted to elucidate the accuracy of the method. The hydrazine concentrations found and the recovery rate are shown in Table 3. The results indicated an excellent hydrazine recovery, and each addition's mean relative standard deviation (R.S.D. %) indicates good reproducibility. Thus, it is suggested that the applicability of the modified electrode was confirmed through a sensitive method for detecting hydrazine in a tap water sample in 0.1 mol L^{-1} KOH solution.

Table 3. Determination of Hydrazine in a Sample with Tap Water in 0.1 mol L^{-1} KOH Solution (n = 3)

sample	spiked	found	recovery (%)	R.S.D. (%)
tap water	24.94	24.37	97.7	6.3
	49.75	50.87	102.3	3.4
	74.44	78.57	105.5	7.2

CONCLUSIONS

This work provides a one-pot synthetic route for the gram-scale production of hierarchical nickel oxide nanoflowers. By morphological and chemical analysis, it was possible to characterize the novel-produced NiO nanoflowers' chemical composition, structure, and morphology. The novel material was dispersed in Nafion and drop-cast onto a glassy carbon surface to produce a modified electrocatalytic platform (NiO NF/GCE). The NiO NF/GCE provided an effective, low-cost, and high-performance alternative for hydrazine's selective and sensitive electrocatalytic sensing. In the presence of hydrazine, it was possible to observe an oxidation overpotential of only +0.08 V vs Ag/AgCl, which ensures a critical behavior for the

Table 2. Comparative Analytical Parameters Obtained for Hydrazine Different Electrochemical Sensors

eletrode modification	overpotential (V)	electrolyte (mmol L^{-1})	linear range (μM)	sensitivity (μA cm^{-2}/mmol L^{-1})	ref
NiO/NF	+0.08 vs Ag/AgCl	KOH 0.1	100−1000	547	this work
[a]$NiCo_2O_4$	+0.36 vs SCE	PBS 0.1	7−1780	48.25	50
[b]$NiCoSe_2$	+0.6 vs Hg/HgO	NaOH 0.1	4−2450	16,170	71
[c]Au/Ti	−0.55 vs Ag/AgCl	NaOH 1.0	5−40,000	1.12	51
[d]Ni-NP	+0.5 vs SCE	NaOH 0.1	1−1300	133	52
[e]ZIF-67/CoAl	+0.87 vs Ag/AgCl	NaOH 0.1	30−1200	4.1	70
[f]C-Cr_2O_3@Ni	+0.4 vs Ag/AgCl	PBS 0.1	0.05−200	918.5	72
[g]Zn-MOF-rGO	+0.42 vs Ag/AgCl	PBS 0.1	0.001−100	540	73

[a]Nickel cobaltite nanoparticles. [b]3D *Setaria viridis*-like $NiCoSe_2$ nanoneedle array. [c]Nanoporous gold particle-modified titanium. [d]β-Nickel hydroxide nanoplatelets. [e]Zeolite imidazole framework-67/cobalt-aluminum-layered double hydroxide. [f]Ni(II)-tannic acid complexes on the lab-made C-Cr_2O_3 nanoparticles. [g]Zinc-metal organic frameworks and reduced graphene oxide.

https://doi.org/10.1021/acsomega.2c07638
ACS Omega 2023, 8, 11978−11986

selective electrochemical determination of this compound. By CV analysis, it was possible to obtain high sensitivity and a low limit of detection, enabling its possible application for environmental monitoring. Amperometric measurements obtained the same conclusions. Also, the material presented a remarkable selectivity and was effective when applied in a real sample. Future efforts can be employed to investigate the electrocatalytic performance of this material for the determination of glucose and hydrogen peroxide as well.

■ ASSOCIATED CONTENT

Supporting Information

The Supporting Information is available free of charge at https://pubs.acs.org/doi/10.1021/acsomega.2c07638.

N_2 adsorption−desorption isotherms, Ip versus potential plot, and amperometry curves (PDF)

■ AUTHOR INFORMATION

Corresponding Authors

Anderson G. M. da Silva − *Departamento de Engenharia Química e de Materiais - DEQM, Pontifícia Universidade Católica do Rio de Janeiro (PUC-Rio), 22453-900 Rio de Janeiro, RJ, Brazil*; Email: agms@puc-rio.br

Marco A. S. Garcia − *Departamento de Química, Centro de Ciências Exatas e Tecnologia, Universidade Federal do Maranhão (UFMA), 65080-805 São Luís, MA, Brazil*; orcid.org/0000-0003-3290-9297; Email: marco.suller@ufma.br

Authors

Rayse M. Ferreira − *Departamento de Química, Centro de Ciências Exatas e Tecnologia, Universidade Federal do Maranhão (UFMA), 65080-805 São Luís, MA, Brazil*

Franciele M. Morawski − *Departamento de Química, Universidade Federal de Santa Catarina (UFSC), 88040-900 Florianópolis, SC, Brazil*

Emanuel C. Pessanha − *Departamento de Engenharia Química e de Materiais - DEQM, Pontifícia Universidade Católica do Rio de Janeiro (PUC-Rio), 22453-900 Rio de Janeiro, RJ, Brazil*; orcid.org/0000-0002-0105-9827

Scarllett L. S. de Lima − *Departamento de Engenharia Química e de Materiais - DEQM, Pontifícia Universidade Católica do Rio de Janeiro (PUC-Rio), 22453-900 Rio de Janeiro, RJ, Brazil*

Diana S. da Costa − *Departamento de Química, Centro de Ciências Exatas e Tecnologia, Universidade Federal do Maranhão (UFMA), 65080-805 São Luís, MA, Brazil*

Geyse A. C. Ribeiro − *Departamento de Química, Centro de Ciências Exatas e Tecnologia, Universidade Federal do Maranhão (UFMA), 65080-805 São Luís, MA, Brazil*

João Vaz − *Departamento de Química, Centro de Ciências Exatas e Tecnologia, Universidade Federal do Maranhão (UFMA), 65080-805 São Luís, MA, Brazil*

Rodolpho Mouta − *Departamento de Física, Universidade Federal do Ceará (UFC), 60455-760 Fortaleza, CE, Brazil*

Auro A. Tanaka − *Departamento de Química, Centro de Ciências Exatas e Tecnologia, Universidade Federal do Maranhão (UFMA), 65080-805 São Luís, MA, Brazil*

Liying Liu − *Centro Brasileiro de Pesquisas Físicas, 22290-180 Rio de Janeiro, RJ, Brazil*

Maria I. P. da Silva − *Departamento de Engenharia Química e de Materiais - DEQM, Pontifícia Universidade Católica do Rio de Janeiro (PUC-Rio), 22453-900 Rio de Janeiro, RJ, Brazil*

Aryane Tofanello − *Center for Natural and Human Sciences (CCNH), Universidade Federal do ABC (UFABC), 09210-170 Santo André, SP, Brazil*

Hector A. Vitorino − *Centro de Investigación en Biodiversidad para la Salud, Universidad Privada Norbert Wiener, Lima 15108, Perú*

Complete contact information is available at: https://pubs.acs.org/10.1021/acsomega.2c07638

Notes

The authors declare no competing financial interest.

■ ACKNOWLEDGMENTS

This work was supported by the Fundação de Amparo à Pesquisa do Estado do Rio de Janeiro (FAPERJ, grant number #E-26/201.315/2021). The authors also acknowledge the financial support from Fundação de Amparo à Pesquisa e ao Desenvolvimento Científico e Tecnológico do Maranhão (FAPEMA, grant INFRA-02264/21) and Coordenação de Aperfeiçoamento de Pessoal de Nível Superior (CAPES, Finance Code 001). A.A.T. acknowledges financial support from FAPEMA (grant UNIVERSAL-01304/19) J.V. also thanks FAPEMA for a PIBIC scholarship (BIC-01913/20). R.M. and J.V. thank the Central Multiusuário de Pesquisa em Materiais e Biossistemas (CeMatBio/UFMA) for X-ray diffraction facilities. LaMAR/UFF was acknowledged for the access of the equipment.

■ REFERENCES

(1) Fiorio, J. L.; Gothe, M. L.; Kohlrausch, E. C.; Zardo, M. L.; Tanaka, A. A.; de Lima, R. B.; da Silva, A. G. M.; Garcia, M. A. S.; Vidinha, P.; Machado, G. Nanoengineering of Catalysts for Enhanced Hydrogen Production. *Hydrogen* **2022**, *3*, 218−254.

(2) Dourado, A. H. B.; da Silva, A. G. M.; Pastrián, F. A. C.; Munhos, R. L.; de Lima Batista, A. P.; De Oliveira-Filho, A. G. S.; Quiroz, J.; De Oliveira, D. C.; Camargo, P. H. C.; de Torresi, S. I. C. In Situ FTIR Insights into the Electrooxidation Mechanism of Glucose as a Function of the Surface Facets of Cu_2O-Based Electrocatalytic Sensors. *J. Catal.* **2019**, *375*, 95−103.

(3) Rodrigues, M. P.; Miguel, V. M.; Germano, L. D.; de Torresi, S. I. C. Metal Oxides as Electrocatalysts for Water Splitting: On Plasmon-Driven Enhanced Activity. *Electrochem. Sci. Adv.* **2022**, *2*, No. e2100079.

(4) Shabri, H. A.; Othman, M. H. D.; Mohamed, M. A.; Kurniawan, T. A.; Jamil, S. M. Recent Progress in Metal-Ceramic Anode of Solid Oxide Fuel Cell for Direct Hydrocarbon Fuel Utilization: A Review. *Fuel Process. Technol.* **2021**, *212*, No. 106626.

(5) da Silva, A. G. M.; Fernandes, C. G.; Hood, Z. D.; Peng, R.; Wu, Z.; Dourado, A. H. B.; Parreira, L. S.; de Oliveira, D. C.; Camargo, P. H. C.; de Torresi, S. I. C. PdPt-TiO_2 Nanowires: Correlating Composition, Electronic Effects and O-Vacancies with Activities towards Water Splitting and Oxygen Reduction. *Appl. Catal., B* **2020**, *277*, No. 119177.

(6) Rodrigues, M. R.; Ferreira, R. M.; Pereira, F.; Silva, F. A.; Silva, A. C. A.; Vitorino, H. A.; Júnior, J. J. G. V.; Tanaka, A. A.; Garcia, M. A. S.; Rodrigues, T. S. Application of AgPt Nanoshells in Direct Methanol Fuel Cells: Experimental and Theoretical Insights of Design Electrocatalysts over Methanol Crossover Effect. *ChemCatChem* **2022**, *14*, No. e202200605.

(7) de Lima, S. L. S.; Pereira, F. S.; de Lima, R. B.; de Freitas, I. C.; Spadotto, J.; Connolly, B. J.; Barreto, J.; Stavale, F.; Vitorino, H. A.; Fajardo, H. V.; Tanaka, A. A.; Garcia, M. A. S.; da Silva, A. G. M. MnO_2-Ir Nanowires: Combining Ultrasmall Nanoparticle Sizes, O-

Vacancies, and Low Noble-Metal Loading with Improved Activities towards the Oxygen Reduction Reaction. *Nanomaterials* **2022**, *12*, 3039.
(8) França, M. C.; Ferreira, R. M.; Pereira, F.; Silva, F. A.; Silva, A. C. A.; Cunha, L. C. S.; Júnior, J. J. G. V.; Neto, P.; Takana, A. A.; Rodrigues, T. S.; Garcia, M. A. S. Galvanic replacement managing direct methanol fuel cells: AgPt nanotubes as a strategy for methanol crossover effect tolerance. *J. Mater. Sci.* **2022**, *57*, 8225−8240.
(9) Lima, C. C.; Fonseca, W. S.; Colmati, F.; Ribeiro, L. K.; França, M. C.; Longo, E.; Garcia, M. A. S.; Tanaka, A. A. Enhancing the methanol tolerance of ultrasmall platinum nanoparticles and manganese oxide onto carbon for direct methanol fuel cell: The importance of the synthesis procedure. *Electrochim. Acta* **2020**, *363*, No. 137256.
(10) Chang, H. W.; Chen, S. C.; Chen, P. W.; Liu, F. J.; Tsai, Y. C. Constructing Morphologically Tunable Copper Oxide-Based Nanomaterials on Cu Wire with/without the Deposition of Manganese Oxide as Bifunctional Materials for Glucose Sensing and Supercapacitors. *Int. J. Mol. Sci.* **2022**, *23*, 3299.
(11) Chen, T. W.; Tamilalagan, E.; Chen, S. M.; Akilarasan, M.; Maheshwaran, S.; Liu, X. An Ultra-Sensitive Electrochemical Sensor for the Detection of Carcinogen Oxidative Stress 4-nitroquinoline N-Oxide in Biologic Matrices Based on Hierarchical Spinel Structured $NiCo_2O_4$ and $NiCo_2S_4$; a Comparative Study. *Int. J. Mol. Sci.* **2020**, *21*, 3273.
(12) Fang, B.; Zhang, C.; Zhang, W.; Wang, G. A Novel Hydrazine Electrochemical Sensor Based on a Carbon Nanotube-Wired ZnO Nanoflower-Modified Electrode. *Electrochim. Acta* **2009**, *55*, 178−182.
(13) Agnihotri, A. S.; Varghese, A.; Nidhin, M. Transition Metal Oxides in Electrochemical and Bio Sensing: A State-of-Art Review. *Appl. Surf. Sci. Adv.* **2021**, *4*, No. 100072.
(14) Pastrián, F. A. C.; da Silva, A. G. M.; Dourado, A. H. B.; de Lima Batista, A. P.; De Oliveira-Filho, A. G. S.; Quiroz, J.; De Oliveira, D. C.; Camargo, P. H. C.; de Torresi, S. I. C. Why Could the Nature of Surface Facets Lead to Differences in the Activity and Stability of Cu_2O-Based Electrocatalytic Sensors? *ACS Catal.* **2018**, *8*, 6265−6272.
(15) Geonmonond, R. S.; da Silva, A. G. M.; Camargo, P. H. C. Controlled Synthesis of Noble Metal Nanomaterials: Motivation, Principles, and Opportunities in Nanocatalysis. *An. Acad. Bras. Cienc.* **2018**, *90*, 719.
(16) da Silva, A. G. M.; Rodrigues, T. S.; Macedo, A.; da Silva, R. T. P.; Camargo, P. H. C. An Undergraduate Level Experiment on the Synthesis of Au Nanoparticles and Their Size-Dependent Optical and Catalytic Properties. *Quim. Nova* **2014**, *37*, 1716−1720.
(17) Xia, Y.; Gilroy, K. D.; Peng, H. C.; Xia, X. Seed-Mediated Growth of Colloidal Metal Nanocrystals. *Angew. Chem. Int. Ed.* **2017**, *56*, 60−95.
(18) Gilroy, K. D.; Ruditskiy, A.; Peng, H. C.; Qin, D.; Xia, Y. Bimetallic Nanocrystals: Syntheses, Properties, and Applications. *Chem. Rev.* **2016**, *116*, 10414−10472.
(19) Yuan, K.; Zhang, Y.; Huang, S.; Yang, S.; Zhao, S.; Liu, F.; Peng, Q.; Zhao, Y.; Zhang, G.; Fan, J.; Zang, G. Copper Nanoflowers on Carbon Cloth as a Flexible Electrode Toward Both Enzymeless Electrocatalytic Glucose and H_2O_2. *Electroanalysis* **2021**, *33*, 1800−1809.
(20) Bhaskar, S.; Rai, A.; Ganesh, K. M.; Reddy, R.; Reddy, N.; Ramamurthy, S. S. Sericin-Based Bio-Inspired Nano-Engineering of Heterometallic AgAu Nanocubes for Attomolar Mefenamic Acid Sensing in the Mobile Phone-Based Surface Plasmon-Coupled Interface. *Langmuir* **2022**, *38*, 12035−12049.
(21) Bhaskar, S.; Singh, A. K.; Das, P.; Jana, P.; Kanvah, S.; Braktha, S.; Ramamurthy, S. S. Superior Resonant Nanocavities Engineering on the Photonic Crystal-Coupled Emission Platform for the Detection of Femtomolar Iodide and Zeptomolar Cortisol. *ACS Appl. Mater. Interfaces* **2020**, *12*, 34323−34336.
(22) Veloso, W. B.; Almeida, A. T. F. O.; Ribeiro, L. K.; de Assis, M.; Longo, E.; Garcia, M. A. S.; Tanaka, A. A.; da Silva, I. S.; Dantas, L. M. F. Rapid and sensitivity determination of macrolides antibiotics using disposable electrochemical sensor based on Super P carbon black and chitosan composite. *Microchem. J.* **2022**, *172*, No. 106939.
(23) de Freitas, I. C.; Parreira, L. S.; Barbosa, E. C. M.; Novaes, B. A.; Mou, T.; Alves, T. V.; Quiroz, J.; Wang, Y. C.; Slater, T. J.; Thomas, A.; Wang, B.; Haigh, S. J.; Camargo, P. H. C. Design-Controlled Synthesis of IrO_2 Sub-Monolayers on Au Nanoflowers: Marrying Plasmonic and Electrocatalytic Properties. *Nanoscale* **2020**, *12*, 12281−12291.
(24) da Silva, A. G. M.; Rodrigues, T. S.; Candido, E. G.; de Freitas, I. C.; da Silva, A. H. M.; Fajardo, H. V.; Balzer, R.; Gomes, J. F.; Assaf, J. M.; de Oliveira, D. C.; Oger, N.; Paul, S.; Wojcieszak, R.; Camargo, P. H. C. Combining Active Phase and Support Optimization in MnO_2-Au Nanoflowers: Enabling High Activities towards Green Oxidations. *J. Colloid Interface Sci.* **2018**, *530*, 282−291.
(25) Aveiro, L. R.; da Silva, A. G. M.; Candido, E. G.; Antonin, V. S.; Parreira, L. S.; Papai, R.; Gaubeur, I.; Silva, F. L.; Lanza, M. R. V.; Camargo, P. H. C.; Santos, M. C. Application and Stability of Cathodes with Manganese Dioxide Nanoflowers Supported on Vulcan by Fenton Systems for the Degradation of RB5 Azo Dye. *Chemosphere* **2018**, *208*, 131.
(26) Shende, P.; Kasture, P.; Gaud, R. S. Nanoflowers: The Future Trend of Nanotechnology for Multi-Applications. *Artif. Cells Nanomed. Biotechnol.* **2018**, *46*, 413−422.
(27) Wei, Z.; Qiao, H.; Zhang, C.; Yan, X. Characterization of NiO nanoparticles by anodic arc plasma method. *J. Alloys Compd.* **2009**, *479*, 855−858.
(28) Chen, D.; Gao, L. A new and facile route to ultrafine nanowires, superthin flakes and uniform nanodisks of nickel hydroxide. *Chem. Phys. Lett.* **2005**, *405*, 159−164.
(29) Justin, P.; Meher, S. K.; Gangavarapu, R. R. Tuning of capacitance behavior of NiO using anionic, cationic, and nonionic surfactants by hydrothermal synthesis. *J. Phys. Chem. C* **2010**, *114*, 5203−5210.
(30) Ding, S.; Zhu, T.; Chen, J. S.; Wang, Z.; Yuan, C.; Lou, X. W. Controlled synthesis of hierarchical NiO nanosheet hollow spheres with enhanced supercapacitive performance. *J. Mater. Chem.* **2011**, *21*, 6602−6606.
(31) Varghese, B.; Reddy, M. V.; Yanwu, Z.; Lit, C. S.; Hoong, T. C.; Rao, G. V. S.; Chowdari, B. V. R.; Wee, A. T. S.; Lim, C. T.; Sow, C. H. Fabrication of NiO nanowall electrodes for high performance lithium ion battery. *Chem. Mater.* **2008**, *20*, 3360−3367.
(32) Wang, B.; Chen, J. S.; Wang, Z.; Madhavi, S.; Lou, X. W. Green Synthesis of NiO Nanobelts with Exceptional Pseudo-Capacitive Properties. *Adv. Energy Mater.* **2012**, *2*, 1188−1192.
(33) Manigandan, R.; Dhanasekaran, T.; Padmanaban, A.; Giribabu, K.; Suresh, R.; Narayanan, V. Bifunctional hexagonal Ni/NiO nanostructures: influence of the core−shell phase on magnetism, electrochemical sensing of serotonin, and catalytic reduction of 4-nitrophenol. *Nanoscale Adv.* **2019**, *1*, 1531−1540.
(34) Kate, R. S.; Khalate, S. A.; Deokate, R. J. Overview of nanostructured metal oxides and pure nickel oxide (NiO) electrodes for supercapacitors: A review. *J. Alloys Compd.* **2018**, *734*, 89−111.
(35) Eder, R. Electronic Structure of NiO: Antiferromagnetic Transition and Photoelectron Spectra in the Ordered Phase. *Phys. Rev. B* **2015**, *91*, No. 245146.
(36) Speck, F. D.; Dettelbach, K. E.; Sherbo, R. S.; Salvatore, D. A.; Huang, A.; Berlinguette, C. P. On the Electrolytic Stability of Iron-Nickel Oxides. *Chem* **2017**, *2*, 590−597.
(37) Smith, R. D. L.; Prévot, M. S.; Fagan, R. D.; Trudel, S.; Berlinguette, C. P. Water Oxidation Catalysis: Electrocatalytic Response to Metal Stoichiometry in Amorphous Metal Oxide Films Containing Iron, Cobalt, and Nickel. *J. Am. Chem. Soc.* **2013**, *135*, 11580−11586.
(38) Xia, C.; Yanjun, X.; Ning, W. Facile synthesis of NiO nanoflowers and their electrocatalytic performance. *Sens. Actuators, B* **2011**, *153*, 434−438.
(39) Mishra, D.; Zhou, R.; Hassan, M. M.; Hu, J.; Gates, I.; Mahinpey, N.; Lu, Q. Bitumen and Asphaltene Derived Nanoporous

https://doi.org/10.1021/acsomega.2c07638
ACS Omega 2023, 8, 11978−11986

Carbon and Nickel Oxide/Carbon Composites for Supercapacitor Electrodes. *Sci. Rep.* **2022**, *12*, 4095.
(40) Zahra, T.; Ahmad, K. S.; Zequine, C.; Gupta, R.; Thomas, A.; Malik, M. A.; Iram, S.; ElBadry, Y. A.; El-Bahy, Z. M. Electrochemical Trapping of Meta-Stable NiO Consolidated ZnO/PdO by Biomimetic Provenance for the Employment of Clean Energy Generation. *Mater. Sci. Semicond. Process.* **2022**, *150*, No. 106867.
(41) Youcef, M.; Hamza, B.; Nora, H.; Walid, B.; Salima, M.; Ahmed, B.; Malika, F.; Marc, S.; Christian, B.; Wassila, D.; Eddine, M. D.; Larbi, Z. A Novel Green Synthesized NiO Nanoparticles Modified Glassy Carbon Electrode for Non-Enzymatic Glucose Sensing. *Microchem. J.* **2022**, *178*, No. 107332.
(42) Trafela, Š.; Zavašnik, J.; Šturm, S.; Rožman, K. Ž. Formation of a $Ni(OH)_2$/NiOOH Active Redox Couple on Nickel Nanowires for Formaldehyde Detection in Alkaline Media. *Electrochim. Acta* **2019**, *309*, 346−353.
(43) Wang, W.; Zhao, Z.; Lei, Q.; Zhang, W.; Li, P.; Zhang, W.; Zhuiykov, S.; Hu, J. Hierarchically Au-Functionalized Derived Ultrathin NiO Nanosheets for Highly Sensitive Electrochemical Hydrazine Detection. *Appl. Surf. Sci.* **2021**, *542*, No. 148539.
(44) Miao, R.; Zeng, W.; Gao, Q. Hydrothermal Synthesis of Novel NiO Nanoflowers Assisted with CTAB and SDS Respectively and Their Gas-Sensing Properties. *Mater. Lett.* **2017**, *186*, 175−177.
(45) Miao, R.; Zeng, W.; Gao, Q. SDS-Assisted Hydrothermal Synthesis of NiO Flake-Flower Architectures with Enhanced Gas-Sensing Properties. *Appl. Surf. Sci.* **2016**, *384*, 304−310.
(46) Yetim, N. K.; Aslan, N.; Sarioğlu, A.; Sari, N.; Koç, M. M. Structural, Electrochemical and Optical Properties of Hydrothermally Synthesized Transition Metal Oxide (Co_3O_4, NiO, CuO) Nanoflowers. *J. Mater. Sci.: Mater. Electron.* **2020**, *31*, 12238−12248.
(47) Qurashi, A.; Zhang, Z.; Asif, M.; Yamazaki, T. Template-Less Surfactant-Free Hydrothermal Synthesis NiO Nanoflowers and Their Photoelectrochemical Hydrogen Production. *Int. J. Hydrogen Energy* **2015**, *40*, 15801−15805.
(48) Winkler, E. L.; Zysler, R. D.; Mansilla, M. V.; Fiorani, D. Surface anisotropy effects in NiO nanoparticles. *Phys. Rev. B* **2005**, *72*, No. 132409.
(49) Yu, Y.; Lee, S. J.; Theerthagiri, J.; Lee, Y.; Choi, M. Y. Architecting the AuPt Alloys for Hydrazine Oxidation as an Anolyte in Fuel Cell: Comparative Analysis of Hydrazine Splitting and Water Splitting for Energy-Saving H_2 Generation. *Appl. Catal. B* **2022**, *316*, No. 121603.
(50) Sudha, V.; Kumar, S. M. S.; Thangamuthu, R. $NiCo_2O_4$ Nanorod: Synthesis and Electrochemical Sensing of Carcinogenic Hydrazine. *Inorg. Chem. Commun.* **2020**, *116*, No. 107927.
(51) Yi, Q.; Yu, W. Nanoporous Gold Particles Modified Titanium Electrode for Hydrazine Oxidation. *J. Electroanal. Chem.* **2009**, *633*, 159−164.
(52) Avanes, A.; Hasanzadeh-Karamjavan, M.; Shokri-Jarcheloo, G. Electrocatalytic Oxidation and Amperometric Determination of Hydrazine Using a Carbon Paste Electrode Modified with β-Nickel Hydroxide Nanoplatelets. *Microchim. Acta* **2019**, *186*, 441.
(53) Yi, Q.; He, J.; Fu, X.; Ying, J.; Gong, L.; Shen, J.; He, X. Carbazole-Based Chemosensor for Highly Sensitive and Selective Bioimaging Identification of Hydrazine in Multiple Model Systems via Ratiometric and Colorimetric. *Dyes Pigm.* **2021**, *196*, No. 109816.
(54) Garrod, S.; Bollard, M. E.; Nicholls, A. W.; Connor, S. C.; Connelly, J.; Nicholson, J. K.; Holmes, E. Integrated Metabonomic Analysis of the Multiorgan Effects of Hydrazine Toxicity in the Rat. *Chem. Res. Toxicol.* **2005**, *18*, 115−122.
(55) Hosseini, S. R.; Ghasemi, S.; Kamali-Rousta, M. Preparation of CuO/NiO Composite Nanofibers by Electrospinning and Their Application for Electro-Catalytic Oxidation of Hydrazine. *J. Power Sources* **2017**, *343*, 467−476.
(56) Ahmad, R.; Bedük, T.; Majhi, S. M.; Salama, K. N. One-Step Synthesis and Decoration of Nickel Oxide Nanosheets with Gold Nanoparticles by Reduction Method for Hydrazine Sensing Application. *Sens. Actuators, B* **2019**, *286*, 139−147.
(57) Adekunle, A. S.; Ozoemena, K. I. Electron Transport and Electrocatalytic Properties of MWCNT/Nickel Nanocomposites: Hydrazine and Diethylaminoethanethiol as Analytical Probes. *J. Electroanal. Chem.* **2010**, *645*, 41−49.
(58) Ci, S.; Huang, T.; Wen, Z.; Cui, S.; Mao, S.; Steeber, D. A.; Chen, J. Nickel Oxide Hollow Microsphere for Non-Enzyme Glucose Detection. *Biosens. Bioelectron.* **2014**, *54*, 251−257.
(59) Tajik, S.; Beitollahi, H.; Hosseinzadeh, R.; Afshar, A. A.; Varma, R. S.; Jang, H. W.; Shokouhimehr, M. Electrochemical Detection of Hydrazine by Carbon Paste Electrode Modified with Ferrocene Derivatives, Ionic Liquid, and CoS_2-Carbon Nanotube Nanocomposite. *ACS Omega* **2021**, *6*, 4641−4648.
(60) Matias, T. A.; de Faria, L. V.; Rocha, R. G.; Silva, M. N. T.; Nossol, E.; Richter, E. M.; Muñoz, R. A. A. Prussian blue-modified laser-induced graphene platforms for detection of hydrogen peroxide. *Microchim. Acta* **2022**, *189*, 188.
(61) Liang, X.; Zhao, Z.; Zhu, M.; Liu, F.; Wang, L.; Yin, H.; Qiu, G.; Cao, F.; Liu, X.; Feng, X. Self-Assembly of Birnessite Nanoflowers by Staged Three-Dimensional Oriented Attachment. *Environ. Sci.: Nano* **2017**, *4*, 1656−1669.
(62) Rietveld, H. M. Line Profiles of Neutron Powder-Diffraction Peaks for Structure Refinement. *Acta Crystallogr.* **1967**, *22*, 151−152.
(63) Grosvenor, A. P.; Biesinger, M. C.; Smart, R. S. C.; McIntyre, N. S. New Interpretations of XPS Spectra of Nickel Metal and Oxides. *Surf. Sci.* **2006**, *600*, 1771−1779.
(64) Saranya, P. E.; Selladurai, S. Mesoporous 3D Network Ce-Doped NiO Nanoflakes as High Performance Electrodes for Supercapacitor Applications. *New J. Chem.* **2019**, *43*, 7441−7456.
(65) Wang, Y.; Cao, F.; Lin, W.; Zhao, F.; Zhou, J.; Li, S.; Qin, G. In Situ Synthesis of Ni/NiO Composites with Defect-Rich Ultrathin Nanosheets for Highly Efficient Biomass-Derivative Selective Hydrogenation. *J. Mater. Chem. A* **2019**, *7*, 17834−17841.
(66) Liu, W.; Lu, C.; Wang, X.; Liang, K.; Tay, B. K. In Situ Fabrication of Three-Dimensional Ultrathin Graphite/Carbon Nanotube/NiO Composite as Binder-Free Electrode for High-Performance Energy Storage. *J. Mater. Chem. A* **2015**, *3*, 624−633.
(67) Golabi, S. M.; Zare, H. R. Electrocatalytic Oxidation of Hydrazine at a Chlorogenic Acid (CGA) Modified Glassy Carbon Electrode. *J. Electroanal. Chem.* **1999**, *465*, 168−176.
(68) Spinner, N.; Mustain, W. E. Effect of Nickel Oxide Synthesis Conditions on Its Physical Properties and Electrocatalytic Oxidation of Methanol. *Electrochim. Acta* **2011**, *56*, 5656−5666.
(69) Han, Y.; Han, L.; Zhang, L.; Dong, S. Ultrasonic Synthesis of Highly Dispersed Au Nanoparticles Supported on Ti-Based Metal-Organic Frameworks for Electrocatalytic Oxidation of Hydrazine. *J. Mater. Chem. A* **2015**, *3*, 14669−14674.
(70) Habibi, B.; Pashazadeh, A.; Pashazadeh, S.; Ali Saghatforoush, L. Electrocatalytic Oxidation and Determination of Hydrazine in Alkaline Medium through in Situ Conversion Thin Film Nanostructured Modified Carbon Ceramic Electrode. *J. Electroanal. Chem.* **2022**, *907*, No. 116038.
(71) Xing, Y.; Tang, X.; Ling, C.; Zhang, Y.; He, Z.; Ran, G.; Yu, H.; Huang, K.; Zou, Z.; Xiong, X. Three-Dimensional Setaria Viridis-like $NiCoSe_2$ Nanoneedles Array: As an Efficient Electrochemical Hydrazine Sensor. *Colloids Surf., A* **2022**, *650*, No. 129549.
(72) Feng, J.; Lang, G.; Li, T.; Zhang, J.; Zhao, J.; Li, W.; Yang, W.; Jiang, Z. Enhanced Electrochemical Detection Performance of C-Cr_2O_3 towards Glucose and Hydrazine by Assembling Ni-MPN Coating. *Appl. Surf. Sci.* **2022**, *604*, No. 154548.
(73) Rani, S.; Kapoor, S.; Sharma, B.; Kumar, S.; Malhotra, R.; Dilbaghi, N. Fabrication of Zn-MOF@rGO Based Sensitive Nanosensor for the Real Time Monitoring of Hydrazine. *J. Alloys Compd.* **2020**, *816*, No. 152509.

https://doi.org/10.1021/acsomega.2c07638
ACS Omega 2023, 8, 11978−11986